Accepted Manuscript online: 2023-12-05 Article published online: 2023-12-15

Recent Advances of Covalent Organic Frameworks as Water Splitting Electrocatalysts

Yusran Yusran‡ [a]
Jie Zhao‡ [b]
Fengqian Chen[a]
Qianrong Fang* [a]

[a] State Key Laboratory of Inorganic Synthesis and Preparative Chemistry, Jilin University, Changchun 130012, P. R. of China
[b] SINOPEC Research Institute of Petroleum Processing, P. R. of China
* qrfang@jlu.edu.cn
‡ These authors contributed equally.

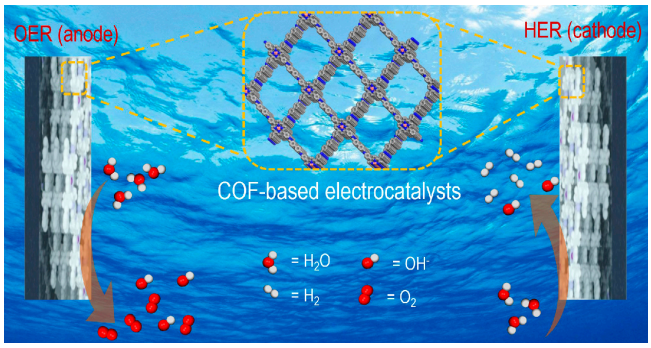

Received: 10.10.2023
Accepted after revision: 28.11.2023
DOI: 10.1055/a-2222-7218; Art ID: OM-2023-10-0009-SR

License terms:

© **2023**. The Author(s). This is an open access article published by Thieme under the terms of the Creative Commons Attribution License, permitting unrestricted use, distribution, and reproduction so long as the original work is properly cited. (https://creativecommons.org/licenses/by/4.0/).

Abstract Developing high-performance, durable, yet low-lost catalysts for electrocatalytic water splitting technology has been a research priority to tackle the global energy crisis. In this regard, covalent organic frameworks (COFs) have received great attention as promising water splitting electrocatalysts as they can provide an excellent platform for the settlement of electrocatalytic active site, high porosity, and good stability. In this review, recent advances on the design and application of COFs for water electrolysis, which are hydrogen and oxygen evolution reaction electrocatalysts, are briefly discussed. Among them, both noble and non-noble metals containing COFs as well as metal-free COF-based electrocatalysts are elaborated. Furthermore, a brief outlook on the development of COFs in the field of water splitting electrocatalysis is provided.

Key words: water splitting, covalent organic frameworks, HER, OER, electrocatalysts

1 Introduction

Developing clean energy conversion and utilization technologies, including batteries/supercapacitors, fuel cells, and water splitting, has been the worldwide focused research to sustainably fulfill the growing global energy demand and also to tackle the serious environmental problems caused by traditional fossil fuels.[1–3] In particular, splitting water into high energy density of hydrogen (H_2) is one of the appealing emission-free energy generation technologies.[4,5] In principle, water splitting involves the dissociation of a water molecule into its components ($2H_2O \rightarrow 2H_2 + O_2$), which is thermodynamically unfavorable and is considered as a combination of a hydrogen evolution reaction (HER) in the cathode and an oxygen evolution reaction (OER) in the anode. Hence, the core task in developing this sustainable and green technology lies in the development of high-performance electrocatalysts to promote these key electrochemical reactions at a lower overpotential.[6] Currently, noble metals such as Pt and Ir/Ru oxides are the benchmark electrocatalysts for HER and OER with favorable reaction kinetics.[7,8] However, the large-scale commercial use of these noble metals is practically challenging due to their high-cost, low selectivity, and poor stability toward corrosion and solvent effects.[9,10] Exploration of cost-effective, highly durable, and conductive catalysts in addition to prominent electrocatalytic activities is highly crucial. To this end, several non-noble metal catalysts have been examined including the earth-abundant metals and their compounds (e.g., perovskite oxides, dichalcogenides, transition metal oxides, metal alloys)[10–14] as well as metal-free carbon materials (graphene, carbon nanotube, nanoporous carbon).[15–17] However, the unpredictable and the poorly defined active sites as well as the required pyrolysis treatment in these materials hinder the controlled structure–activity relationships, thus greatly affecting the understanding of the reaction mechanisms. Furthermore, as the electrochemical reaction occurs on the electrode surface while the charges wander through the void, the low porosity of those catalysts could lead to inefficient electrocatalytic performances.

To tackle the aforementioned drawbacks, continuous endeavors on the design of new kind of electrocatalysts for water electrolysis have been advanced in the recent decades.[6] In particular, the discovery of crystalline porous covalent organic frameworks (COFs) by Yaghi and team[18] has opened a new horizon in the development of a non-precious water splitting electrocatalyst. COFs offer an unprecedented set of important features to promote the electrochemical processes such as a well-tuned chemical composition, high structural order, as well as high porosity.[19,20] In addition to high chemical stability as reinforced by covalent linkages,

Biosketches

Yusran Yusran received his B.Sc. (2012) in chemistry from State University of Makassar, Indonesia and M.Sc. (2014) in chemistry from Gadjah Mada University, Yogyakarta, Indonesia. He earned his PhD (2020) in inorganic chemistry from Jilin University, China in 2020 under supervision of Prof. Qianrong Fang and Prof. Shilun Qiu. During 2020 – 2022, he worked with Prof. Zhanting Li as a postdoctoral fellow in the Department of Chemistry, Fudan University, China. He is now joining Prof. Qianrong Fang as a Dingxin postdoctoral fellow in the Chemistry Department of Jilin University, China. His current research focuses on design and synthesis of covalent organic frameworks (COFs) and their potential application in catalysis and energy storage.

Jie Zhao received his doctor's degree of chemical technology from Tianjin University, and studied at the University of California-Riverside as a joint PhD student. He is now working in Research Institute of Petroleum Processing, Sinopec as the director of Fuel and Lubricant Research Department, specializing in the research and development of jet fuel and related additives. He also dedicated in standardization of petroleum and related products.

Fengqian Chen received his B.Sc. from Yanbian University in 2018. He earned his PhD in inorganic chemistry from Jilin University, China in 2023 under supervision of Prof. Qianrong Fang. He is now joining Prof. Qianrong Fang as a postdoctoral fellow in chemistry department of Jilin University, China. His current research interests focus on the synthesis and application of covalent organic frameworks (COFs).

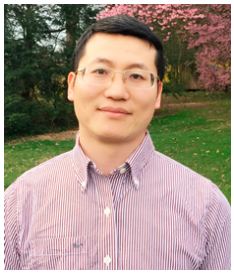

Qianrong Fang received his B.Sc. (2001) and PhD (2007) from Jilin University in China. From 2007 to 2014, he completed his postdoctoral study in University of California at Los Angeles, Texas A&M University, University of California at Riverside as well as University of Delaware. In 2015, he went back to the State Key Laboratory of Inorganic Synthesis & Preparative Chemistry at Jilin University as a full professor. His current research focuses on the design and synthesis of covalent organic frameworks (COFs) for applications in adsorption, separation, catalysis, and a number of others.

the modular incorporation of electroactive components into the structures provides accessible catalytic sites.[21–23] Moreover, COFs can be designed with fully/improved π-conjugated structures, showing semiconducting behavior and well-tuned electronic band gaps.[24–27] All these attractive features show great promises as an attractive electrocatalyst, an alternative to noble-metal electrodes. Hence, although COF research in electrochemical devices is still in its infancy, this new material has also been explored recently for advancing the water splitting electrocatalysis. This review aims to briefly discuss the recent advancements of COF electrocatalysts in water splitting, including the design strategy as well as their electrocatalytic performances. Finally, a brief outlook on developing COF-based catalysts for this green energy conversion is provided.

2 Principle of Water Splitting

Water splitting is one of the important clean energy technologies and is the major source of hydrogen, the highest gravimetric energy density fuel. This electrochemical technology is a combination of two half-reactions: HER and OER.[28,29] Furthermore, it is considered as an environmentally friendly way for large-scale H_2 production in comparison with the existing methods (e.g., steam reforming). In particular, splitting a water molecule into hydrogen (H_2, HER) and oxygen (O_2, OER) molecules is a sluggish chemical process, which, in principle, requires a thermodynamic voltage of 1.23 V (at 25 °C). Moreover, kinetics of these electrochemical reactions significantly influence the output performance of the energy conversion devices. Specifically, due to the resistances and the intrinsic activation barriers present on electrodes, a much higher voltage than the standard thermodynamic voltage is generally required. This excess potential needed is known as overpotential (η). To minimize this overpotential and to achieve as high a current density as possible, a powerful electrocatalyst is thus applied, which is the central issue of the development of prominent water splitting. On the other hand, there are some indicators that have been set to appraise the electrocatalyst performance in water splitting, including current density (j), Tafel slope (b), electrocatalyst stability, and Faradaic efficiency. Current density defines the electrocatalyst activity, which is expressed as either $mA \cdot mg^{-1}$ (normalized to electrode mass) or $mA \cdot cm^{-2}$ (normalized to electrode geometric area) under an applied potential. The Tafel slope, in particular, expresses the catalytic mechanisms for the electrode reactions, which is obtained from the slope of the Tafel plot ($\eta = b \log(j) + a$). The stability determines the practical adaptability of an electrocatalyst that can be examined by both chronoamperometry and chronopotentiometry. Meanwhile, Faradaic efficiency describes the charge efficiency in which the electrons are utilized to form hydrogen. The electrocatalyst should be able to optimize those indicators, requirements that are always under research focuses.

2.1 Hydrogen Evolution Rection

The H_2 evolution is a multistep two-electron transfer reaction involving the adsorption of hydrogen/water, reduction of dihydrogen and desorption of the formed intermediate either in acidic or alkaline media. These steps can be classified as a Volmer step, in which the adsorption of hydrogen on the catalyst surface takes place (eq. 1 and 2) during the reduction of protons. Meanwhile, through either the Heyrovsky step (eq. 3 and 4) or the Tafel step (eq. 5 and 6), molecular H_2 will be formed by the combination of H* species (the * indicates the active sites on the catalyst surface and H* is the absorbed hydrogen). Thus, to evolute H_2 from the reduction of protons/water on the catalytic sites in an acidic electrolyte, for example, HER may occur through either the Volmer–Heyrovsky or Volmer–Tafel path. Meanwhile, in basic solutions, the protons are in the form of water molecule and thus the discharge species will be H_2O to form the H* and H–O bonds by releasing OH^- to the electrolyte. In particular, Pt is regarded as benchmark catalyst for unbeatable electrocatalytic HER and has an extremely high exchange current density and a small Tafel slope.[30]

Volmer step

$^* + H^+ + e^- \rightarrow H^*$ (acidic) (eq. 1)

$^* + H_2O + e^- \rightarrow H^* + OH^-$ (alkaline) (eq. 2)

Heyrovsky step

$H^+ + e^- + H^* \rightarrow H_2 + ^*$ (acidic) (eq. 3)

$H_2O + e^- + H^* \rightarrow H_2 + OH^- + ^*$ (alkaline) (eq. 4)

Tafel step

$2H^* \rightarrow H_2 + 2^*$ (acidic) (eq. 5)

$2H^* \rightarrow H_2 + 2^*$ (alkaline) (eq. 6)

2.2 Oxygen Evolution Rection

The electrochemical O_2 evolution, the other half-reaction in water splitting, is a four-electron transfer reaction and struggles even more with its kinetically sluggish nature and a high overpotential. The OER mechanism is sensitive toward structure of the electrode surface, material types, and involves several intermediate species such as OH*, OOH*, and O* that are produced during reaction and react to generate O_2 (eq. 7 and 8).[28] This complicated mechanism causes more critical steps that need to be considered in both acidic and basic solutions, as it involves the breaking of H–O bonds and subsequent formation of O=O bonds. Despite its high cost and scarcity, RuO_2 has been the benchmark catalyst for OER with an overpotential as small as 420 mV compared to other noble-metal oxides.[31] However, RuO suffers from chemical instability, especially in acidic solutions at a high anodic potential (> 1.4 V).[32]

Acidic condition: $2H_2O \rightarrow O_2 + 4H^+ + 4e^-$ (eq. 7)

Mechanism:

$^* + H_2O \rightarrow OH^* + H^+ + e^-$

$OH^* \rightarrow O^* + H^+ + e^-$

$2O^* \rightarrow 2^* + O_2$

$O^* + H_2O \rightarrow OOH^* + H^+ + e^-$

$OOH^* \rightarrow O_2 + H^+ + e^-$

Basic condition: $4OH^- \rightarrow 2O_2 + 2H_2O + 4e^-$ (eq. 8)

Mechanism:

$^* + OH^- \rightarrow OH^* + e^-$

$OH^* + OH^- \rightarrow O^* + H_2O + e^-$

$2O^* \rightarrow 2^* + O_2$

$O^* + OH^- \rightarrow OOH^* + e^-$

$OOH^* + OH^- \rightarrow O^* + O_2 + H^+ + e^-$

3 COF-Based Water Splitting Electrocatalysts

3.1 Potential COFs as Water Splitting Electrocatalysts

As an emerging crystalline porous polymer, COFs have found great applications in electrocatalysis. In particular, for a decent electrocatalyst, it should show favorable catalytic activity, desired selectivity, and yet good durability. In this regard, with controllable synthesis and predictable properties,[24] COFs are expected to fulfill these criteria. COFs are constructed from predesigned building units with a variety of chemical compositions and electroactive functionals to create rigid and electroactive porous polymers.[22] Moreover, several COFs exhibited some intriguing characteristics, such as high specific surface areas (up to 4210 $m^2 \cdot g^{-1}$), tunable pore sizes (up to 4.7 nm), exceptional thermal (up to 600 °C) and chemical stabilities, and high charge mobility (up to 8.1 $cm^2 \cdot V^{-1} \cdot s^{-1}$).[19,33,34] As a result, COFs provide fully exposed and accessible catalytic active sites which are crucial to improve the efficiency, selectivity, and to reduce reaction energy barrier. Furthermore, the presence of nano-to-mesoporous channels serves as effective electron-transfer and mass-transport pathways and also enables the effective confinement of single atoms, nanoparticles, and nanocluster electrocatalysts. In addition, the π-conjugated structures in most of COFs contribute to the electronic conductivity, which can facilely be improved by heteroatom incorporation, dopant control, and chemical environment manipulation.[16] More importantly, the reticular synthesis of COFs provides insight into the structure–activity relationship, which is pivotal to provide understanding of the electrocatalytic mechanism and modulation. All these critical properties lead to promising application as water splitting electrocatalysts.

3.2 COF-Based HER electrocatalysts

Although COFs in general possess low intrinsic conductivity and moderate stability under electrocatalytic conditions, a number of 2D/3D COFs haven been explored as great alternative HER electrocatalysts (Table 1). The first effort in exploring COFs as an HER electrocatalyst was reported by Pradhan and co-workers in 2017.[35] The team synthesized an electroactive quasi-2D COF (SB-PORPy) via a Schiff-base condensation reaction of a porphyrin (5,10,15,20-tetrakis-(4-aminophenyl)porphyrin, TAP) with a pyrene (1,3,6,8-tetrakis(4-formyl-phenyl)pyrene, TFFPy) building unit to afford a square-like pore COF (Figure 1a). SB-PORPy exhibited a high Brunauer–Emmett–Teller (BET) surface area of 869 $m^2 \cdot g^{-1}$ with an accessible pore width of 1.8 nm (Figure 1b). The idea of stitching porphyrin and pyrene units could give rise to a conducting channel derived from the π electronic conjugation of the AA layer stacking mode. Furthermore, the N-imine (-C=N-) species in the SB-PORPy were considered as perfect free-docking sites for HER upon protonation, forming positive hyperporphyrinic sites. Accordingly, SB-PORPy was employed as an electrocatalyst for HER by mechanically grinding it (2 mg) with carbon-black (1 : 1 weigh ratio) in 0.5 M H_2SO_4 aqueous solution. Remarkably, the SB-PORPy-based electrode exhibited high current density and an overpotential of 380 mV at 5 $mA \cdot cm^{-2}$ for HER, much lower than other reported metal-free COFs, as well as Vulcan and bare glassy carbon electrodes (Figure 1c). Although additional carbon-black is required to improve conductivity, the results of this work thus imply the potential use of metal-free COFs as HER electrocatalysts. Furthermore, the Tafel slope obtained from the polarization curve was about 116 $mV \cdot dec^{-1}$, indicating that the hydrogen evolution mechanism followed the Volmer–Heyrovsky pathway in which the H–H combination was driven by the help of other adjacent imine nitrogen sites to evolute hydrogen from the surface (Figure 1d). More importantly, the electrode shows decent electrocatalytic stability even after 500 cycles with negligible change in terms of both onset potential and current density at a scan rate of 100 $mV \cdot s^{-1}$. This work, as the first case, inspires that metal-free HER electrocatalysts can be designed by simply reticulating an electroactive component into COFs. More advanced achievement was reported by Li and co-workers in 2019, in which the team developed a free-standing 2D conjugated (C–C linked) COF film (2DCCOF1) as a metal-free COF HER electrocatalyst.[37] The 2DCCOF1 film was prepared by Suzuki coupling polymerization on a water–toluene interface in 1,4-bis (4,4,5,5-tetramethyl-1,3,2-dioxaborolan-2-yl)benzene with 1,3,5-triiodobenzene to afford a C–C linked 2DCCOF1 film in the presence of $Pd(PPh_3)_4$ as a catalyst. The resultant thin film possessed millimeter lateral size and its crystalline domain can be visualized under high-resolution transmission electron microscopy. Structurally, 2DCCOF1 was a layered graphene analogue with homogeneous pore[53], making it a potential material for energy storage and optoelectronic applications. Subsequently, 2DCCOF1 was deposited horizontally on the copper electrode. Notably, the 2DCCOF1 film exhibits excellent HER activity compared with that of bare copper electrode with an overpotential of 541 mV (at 10 $mA \cdot cm^{-2}$) and a Tafel slope of 130 $mV \cdot dec^{-1}$. Hence, it is assumed that HER active sites arise from the good electronic conductivity and the well-arranged graphitic-like structure of the 2DCCOF1 film.

Although metal-free HER electrocatalysts are low cost and attractive, their performances are still insufficient. To this end, incorporation of electroactive metals into COFs has also been performed to improve the electrocatalytic performance of the pristine COFs or act as HER active sites. In particular, as for earth-abundant elements and good electroactivity, transition metals are highly potential electrocatalysts.[54] Villagrán and co-workers in 2018 synthesized cobalt

Table 1 Tabulated COF-based water splitting electrocatalysts

COF-based electrocatalysts	Electrocatalytic system	Surface areas[a]/pore size ($m^2 \cdot g^{-1}$/nm)	Electrode active mass ($mg \cdot cm^{-2}$)	η (mV, at 10 $mA \cdot cm^{-2}$)	b ($mV \cdot dec^{-1}$)	Ref.
Metal-free COFs						
SB-PORpy	HER	869/1.8	–	380[b]	116	35
PY-SE-COF	HER	998.03/2.64	–	–	263	36
2DCCOF1 film	HER	–/–	–	541	130	37
BPT-COF-rGO	HER	–/–	–	45	53	40
H_2PcCOF	OER	467/1.2	3	>430	121	45
IISERP-COF3	OER	2022/2.5	5[d]	400	–	49
Tp-Tta COF	OER	716/1	1	430	129	50
C4-SHz COF	OER	1224/1.85	0.07	320	39	51
JUC-630	OER	907/2.35	–	400	104	52
Metal-containing COFs						
CoTcPP	HER	441.74/–	0.08	475	–	29
PY-SE-COF-Pd	HER	717.73/2.64	–	128	150	36
Ru@COF-1	HER	912/1.7	–	200	140	38
c-CNT@TpBpy-Ru	HER	–/–	0.5	112	–	39
Co-TpBpy	OER	450/–	–	400[c]	59	41
Macro-TpBpy-Co	OER	387/–	0.25	380	54	42
CoTAPP-PATA-COF	OER	943.72/1.1	0.2	420	56	43
CoTAPP-BDTA-COF	OER	1047.82/1.2	0.2	470	57	43
NiTAPP-PATA-COF	OER	–/–	0.2	670	–	43
FeTAPP-PATA-COF	OER	–/–	0.2	550	–	43
ZJTU-1@Co	OER	656.8/0.51	4	295	63	44
H_2NiPcCOF	OER	462/1.3	3	430	68	45
NiPcCOF	OER	323/1.3	3	410	75	45
H_2FePcCOF	OER	326/1.4	3	430	62	45
H_2FeNiPcCOF	OER	346/1.4	3	430	78	45
$Ni_{0.5}Fe_{0.5}$@COF-SO_3	OER	281/1.2	–	300	83	46
COF-TpDb-TZ-Co	OER	–/–	–	390	82	47
Co_xNi_y-IISERP-COF2	OER	~161.5/–	20[d]	258	39.8	48
Ni_3N-IISERP-COF3	OER	~606/~2	0.07	230	79	49
Fe-SAC@COF	OER	716/1	1	290	40	50
Ni-SAC@COF	OER	~716/~1	1	337	45	50
Fe-NP/COF	OER	~716/~1	1	359	51	50

Note: [a]Based on the Brunauer–Emmett–Teller (BET) method. [b]Measured at a current density of 5 $mA \cdot cm^{-2}$. [c]Measured at a current density of 1 $mA \cdot cm^{-2}$. [d]Electrode active mass indicated as μg; – = data are unavailable.

porphyrin-based crystalline polymeric materials for electrocatalytic HER.[29] The polymer was prepared by polymerization of a metalloporphyrin-based CoTcPP (TcPP: meso-tetra (4-carboxyphenyl)porphyrin) and exhibited crystalline feature as confirmed by powder X-ray diffraction (PXRD) analysis and showed a moderate specific surface area of 441.74 $m^2 \cdot g^{-1}$. As metalloporphyrin shows improved activity in biological systems and chemical catalysis,[55,56] this inspires other authors to employ CoTcPP as an HER electrocatalyst in acidic 0.5 M H_2SO_4 aqueous solution. As predicted, an electrode composed of CoTcPP (mass loading of 0.08 $mg \cdot cm^{-2}$) showed HER activity with an overpotential of 475 mV (deposited on FTO glass slides), which was smaller than that of its discrete CoTcPP molecule (666 mV) at 10 $mA \cdot cm^{-2}$ cathodic current density. This electrocatalytic activity may arise from the existence of a porous channel to access the metalloporphyrin active sites. The results identify that stitching an electroactive component into a repetitive structure improved the catalytic activity. On the other hand, inspired by remarkable chemical stability of vinylene-linked COFs,[57] this type of COFs is highly interesting as a host for immobilization of metal-based electrocatalysts. In this regard, Pd(II) has been deposited on the pore wall of vinylene-linked PY-SE-COF as a non-platinum electrocatalyst for

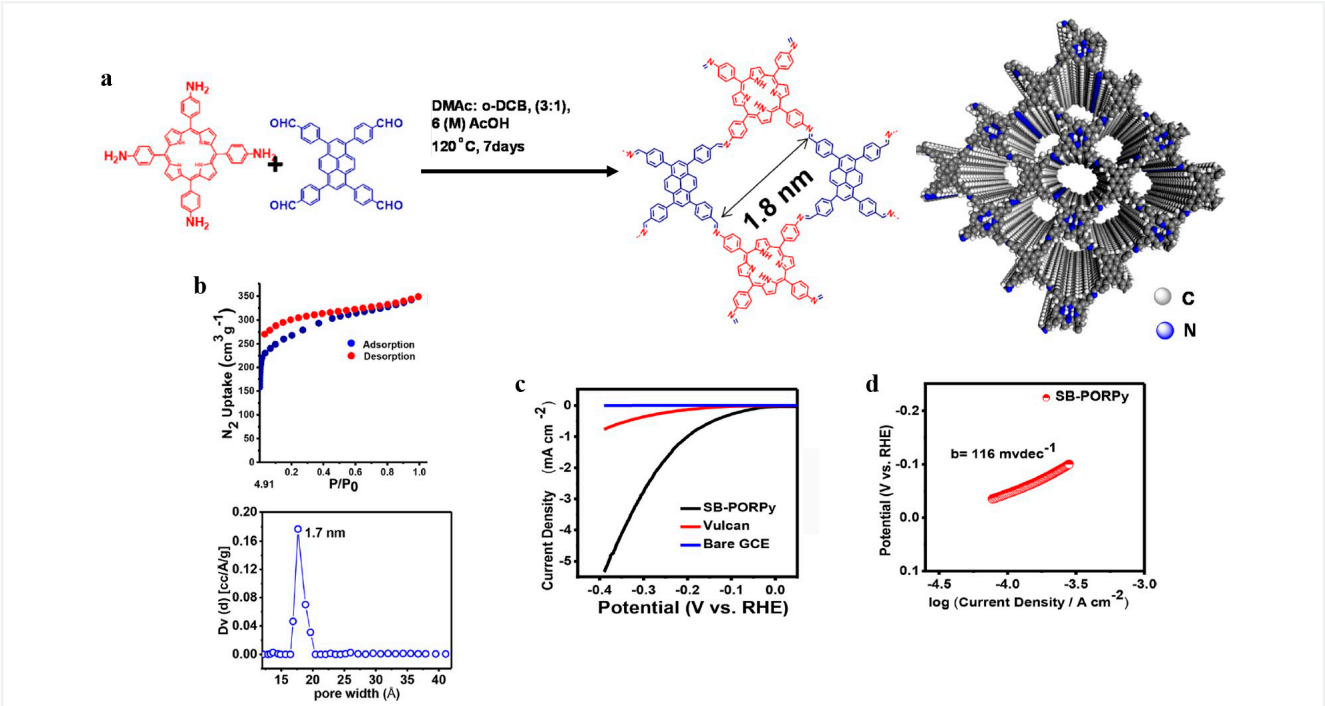

Figure 1 The synthesis and HER electrocatalytic performance of SB-PORPy. (a) Solvothermal synthesis of SB-PORPy and its representative 3D structural model. (b) The N_2 adsorption isotherm and pore size distribution of SB-PORPy. (c) Polarization curves for the HER on bare GCE (blue), Vulcan (red), and SB-PORPy-COF (black) electrodes. (d) Tafel plot of the SB-PORPy-COF electrode. Adapted with permission from Ref. 35. Copyright 2017 American Chemical Society.

HER.[36] The PY-SE-COF was prepared through Knoevenagel condensation of 1,3,6,8-tetrakis(4-formylphenyl)pyrene (TFPPY) with 4,4′-(benzoselenadiazole-4,7-diyl) diacetonitrile (SEA), affording a high crystalline square-like 2.64 nm mesoporous 2D COF with surface areas reaching 998.03 $m^2 \cdot g^{-1}$. The presence of abundant coordinating sites of N and Se in selenodiazole modules render PY-SE-COF as a perfect host to accommodate Pd (II) ions. The loading of Pd into the COF (PY-SE-COF-Pd) can reach 16.8 wt% with minimum reduction of surface areas (717.73 $m^2 \cdot g^{-1}$) and negligible change of pore size. Notably, PY-SE-COF-Pd exhibited a small overpotential of 128 mV at a current density of 10 $mA \cdot cm^{-2}$ when employed as a HER electrocatalyst in an acidic electrolyte (0.5 M H_2SO_4), outstanding in comparison with the performance of individual PY-SE-COF and $PdCl_2$ (240 mV). Furthermore, PY-SE-COF-Pd exhibited a Tafel slop of 150 $mV \cdot dec^{-1}$, much smaller than those of individual PY-SE-COF (263 $mV \cdot dec^{-1}$) and $PdCl_2$ electrodes (245 $mV \cdot dec^{-1}$). These results clearly identify that the improved HER activity arises from the collective electrocatalytic capability of each component. More intriguingly, the high chemical stability of the host leads to the only slight decrease current density even after 2000 CV cycles.

Pristine COFs and transition metal-incorporated COFs offer low-cost HER. However, their performances are still lower than those of noble-metal electrocatalysts. To this end, immobilization of noble metals into COFs has been an attractive avenue for construction of powerful HER electrocatalysts, yet improved catalyst stability toward corrosion under acidic conditions. Chen and team took advantage of the excellent chemical stability of vinylene-linked COFs and the good electrical conductivity of triazine-containing COFs when protonated as a perfect host to immobilize a Ru noble metal catalyst (Figure 2).[38] The vinylene-linked COF-1 was prepared by reacting 2,4,6-trimethyl-1,3,5-triazine (TMTA) with 1,4-diformylbenzene (DFB) in the presence of KOH as a catalyst (Figure 2a). The resultant 2D COF-1 was highly crystalline with a high specific surface area of 1140 $m^2 \cdot g^{-1}$ and established a pore channel of 1.84 nm, making it attractive for noble metal immobilization (Figure 2b). Intercalation of Ru metal (7.5 wt%) at room temperature afforded a Ru@COF-1 composite with minimum reduction of both surface areas and pore size (down to 912 $m^2 \cdot g^{-1}$ and 1.7 nm, respectively). The presence of Ru (III) ion and the significantly retained porosity and crystallinity render the Ru@COF-1 composite promising as a HER electrocatalyst, facilitating full contact between reactants and catalytic sites. As a result, the Ru@COF-1 electrode afforded a small overpotential of 200 mV at 10 $mA \cdot cm^{-1}$ in an acidic electrolyte (0.5 M H_2SO_4), smaller than that of $RuCl_3$, while COF-1 was inactive for HER electrocatalysis (Figure 2c). This result justifies that the Ru (III) ion was the main HER active site and COF-1 im-

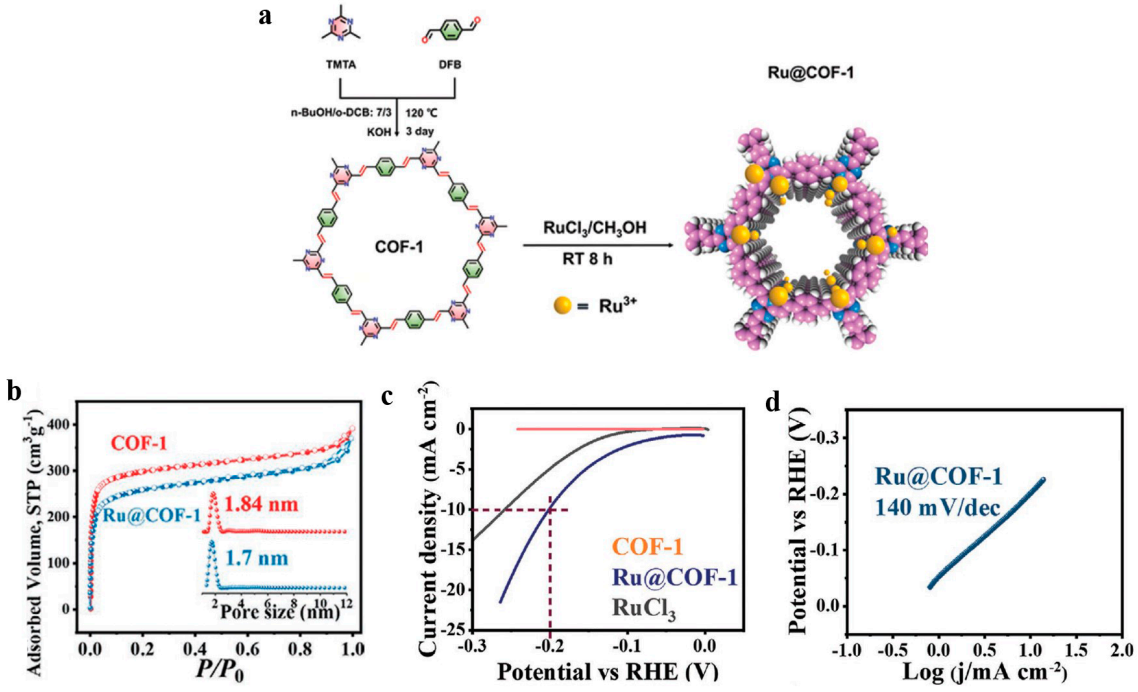

Figure 2 Design synthesis of noble metal-based Ru@COF-1 HER electrocatalysts. (a) Synthetic route to COF-1 and Ru@COF-1 composite. (b) N_2 adsorption isotherm curves and the pore size distributions of COF-1 and Ru@COF-1. (c) Linear sweep voltammetry (LSV) curves toward HER of $RuCl_3$, COF-1, and Ru@COF-1. (d) Tafel plot of Ru@COF-1. Reprinted with permission from Ref. 38. Copyright 2022 Wiley-VCH.

proves the performance by confinement. Furthermore, Ru@-COF-1 exhibited a Tafel slope of 140 $mV \cdot dec^{-1}$, thus the HER mechanism follows the Volmer path as a rate-determining step (Figure 2d). As predicted, Ru@COF-1 showed impressive durability even after 1000 CV cycles, proving the structural stability of the host and the strong coordination bond among Ru ions and COF-1.

Incorporation of metal nanoparticles (M NPs) into porous COFs has also been adapted to diversify COF-based HER electrocatalysts. In particular, covalent triazine frameworks (CTFs), a class of chemically stable COFs, are attractive hosts for accommodating metals or M NPs as their triazine (C_3N_3) units would allow for facile charge transfer and act as additional HER active sites.[58,59] Hu and team designed a CTFs/MoS_2 composite as HER electrocatalysts by in situ growing MoS_2 NPs into the pore surface of a CTF.[60] The CTF was prepared via traditional ionothermal synthesis in the presence of $ZnCl_2$ in a vacuum Pyrex tube under N_2 atmosphere. The CTF afforded high surface areas as large as 1562.6 $m^2 \cdot g^{-1}$ and a homogeneous pore diameter of 1.1 nm. Subsequently, the CTF was soaked into a solution containing $(NH_4)_6Mo_7O_{24}.4H_2O/CH_4N_2S$ and further transferred to hydrothermal treatment to afford CTF/MoS_2-*X* composites with a controlled quantity of NP loading (*X* = CTF/MoS_2 mass ratio = 0.1, 0.2, 0.5, 1, 2, 5, 10). The large surface areas and accessible pore size lead to the nanosized-to-large NP growth of MoS_2 in the pore surface of the CTF, thus exposing more catalytic sulfur edge for HER.[61] Remarkably, the CTFs/MoS_2-5 composite with surface areas and pore volume of 131.8 $m^2 \cdot g^{-1}$ and 0.19 $cm^3 \cdot g^{-1}$, respectively, exhibited an overpotential of 93 mV at a current density of 10 $mA \cdot cm^{-1}$ in an acidic electrolyte (0.5 M H_2SO_4) for HER, which was much smaller than those of CTFs (409 mV) and free MoS_2 (407 mV)-based electrodes. Indeed, the overpotential of CTFs/MoS_2-5 was almost comparable to that of the Pt benchmark catalyst (20% Pt/C). This notable electrocatalysis performances were assumed due the presence of well-arranged 1D channel arrays allowing effective electron transmission and mass diffusion as well as the accessibility of MoS_2 active sites in the H_2 evolution process.

Electron transfer is crucial in the electrocatalytic process. Depositing COFs on conductive materials (graphene, carbon nanotubes, etc.) could improve the electric conductivity of the hybrid materials and accelerate the electron transfer. Recently, Liu and team developed a strategy to better exploit the potential use of COFs as HER electrocatalysts by growing a chemically stable COF film onto the electrically conductive graphene oxide (GO) to afford a COF-GO membrane-based electrocatalyst (Figure 3).[40] The highly π-conjugated aza-fused BPT-COF was prepared by a liquid-phase method of a dilute solution containing 2,3,6,7,10,11-triphenylenehexaamine (TPHA) and 2,7-di-*tert*-butylpyrene-4,5,9,10-tetrone

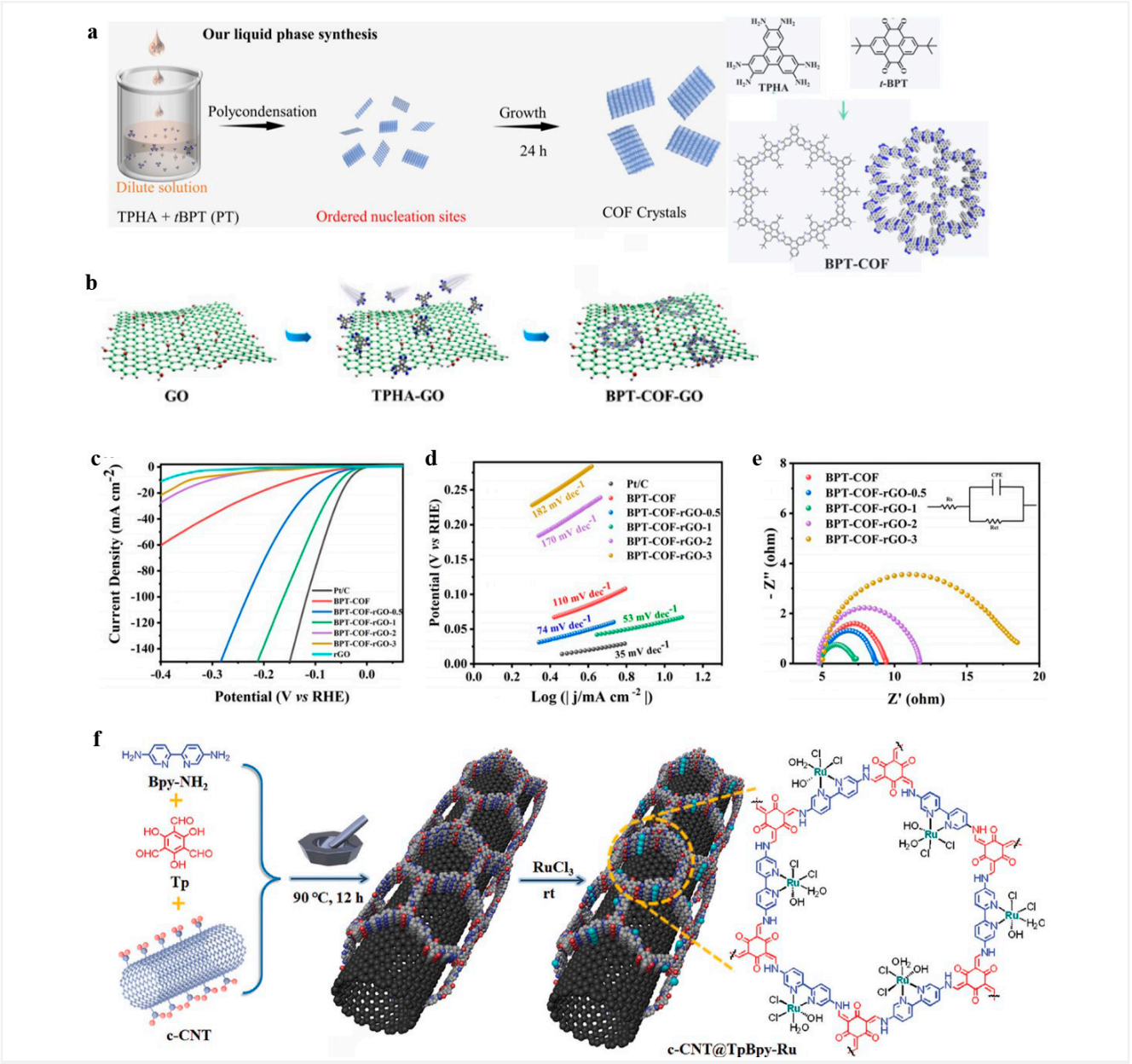

Figure 3 Design synthesis of COF/conductive substrate composites for enhanced electrocatalytic HER performance. (a) Schematic illustration of aza-fused BPT-COF synthesis by a solvothermal or liquid-phase method. (b) Schematic illustration of the fabrication of BPT-COF-GO electrode. (c) LSV curves of Pt/C, BPT-COF, BPT-COF-rGO-*x* (*x* = 0.5, 1, 2, 3), and rGO in 0.5 M H_2SO_4. (d) The related Tafel plots of BPT-COF-rGO membranes. (e) The Nyquist plots of the BPT-COF-rGO membranes. Reprinted with permission from Ref. 40. Copyright 2021 Wiley-VCH. (f) Synthesis route for c-CNT@TpBpy-Ru HER electrocatalyst. Reprinted with permission from Ref. 39. Copyright 2023 Wiley-VCH.

(*t*-BPT) at room temperature in an open system (Figure 3a). This strategy allows for spontaneous polycondensation of both vicinal diamines and diketones driven by near-equilibrium film growth. Adopting this strategy, a uniform COF film was in situ assembled with a conducting GO substrate by dissolving a TPHA/GO mixture and the composite membrane was obtained via vacuum filtration (BTP-COF-GO hybrid membrane) (Figure 3b). This hybrid membrane was then reduced by annealing to obtain conductive BTP-COF-rGO and further loaded onto a glassy carbon electrode. Remarkably, the BPT-COF-rGO-*x* membrane (*x* = mass ratio of GO to TPHA = 1) achieved very small overpotential (45 mV) for HER at 10 $mA \cdot cm^{-1}$ in an acidic electrolyte (0.5 M H_2SO_4), which was better than those of metal-free and met-

al-based HER electrocatalysts mentioned earlier and also close to that of the 20% of the commercial Pt/C catalyst (34 mV) (Figure 3c). Furthermore, it exhibited a small Tafel slope of 53 $mV \cdot dec^{-1}$, which was lower than that of N-doped graphene, thus indicating that the Heyrovsky reaction is the rate-determining step in the electrocatalytic HER process (Figure 3d).[6] Furthermore, BPT-COF-rGO-1 demonstrated efficient charge transfer with very small resistance (2.5 Ω) according to the Nyquist plot (Figure 3e). All these results confirmed the critical role of the chemical and electronic coupling of both the COF membrane and the conductive rGO substrate. Meanwhile, adopting a similar strategy, Wang and team reported an elegant strategy by grafting the ruthenium (Ru)-modified bipyridine-based COF (TpBpy-Ru) on carboxyl-functionalized carbon nanotubes (c-CNTs), thus enhancing the electron transfer capacity (Figure 3f).[39] The c-CNT@TpBpy was firstly prepared via mechanochemical grinding and further immobilizing the Ru precursor at room temperature. Such a synthetic strategy combines the well-dispersed HER active Ru species on TpBpy pores and enhanced the electron transfer capacity of the c-CNT@TpBpy composite. Benefited from the retained crystallinity and porosity, the c-CNT-0.68@TpBpy-Ru electrode (mass loading 0.5 $mg \cdot cm^{-2}$) showed excellent HER activity with an overpotential 112 mV (at 10 $mA \cdot cm^{-2}$) and a remarkable stability for 12 h in 1.0 M KOH, which is superior to those of most of the reported COF electrocatalysts in alkaline solution.

So far, all these reported COF-based HER electrocatalysts are promising. However, their electrocatalytic performances in general are still lower than those of benchmark catalysts. The poor electrical conductivity and the lower chemical stability, especially under harsh electrochemical conditions of most of COFs, are the major obstacles for achieving desirable practical application for water electrolysis.

3.3 COF-Based OER Electrocatalysts

OER, the other half-reaction in a water electrolysis system, has a similar importance to HER but undergoes at a more complex and sluggish rate. In particular, OER involves the intervention of multiple protons and electrons, thus metals with variable oxidation states are necessary as oxygen evolving catalysts.[62] Unfortunately, those metal catalysts particularly suffer from dissociation into a soluble homogeneous species during the catalytic operation,[63] thus incorporation into a highly stable support is highly necessary. To this end, COF materials have also been manipulated for electrocatalytic OER due to their prominent properties for settlement of electroactive metals on the pore surface (Table 1).[21,22] The first effort in realizing COFs for OER was reported by Kurungot and team in 2016, using a cobalt (Co)-containing 2D COF (Figure 4).[41] The COF was obtained by Schiff-base condensation of a 1,3,5-trifomylphloroglucinol (Tp) with 2,2′-bipyridine-5,5′-diamine (Bpy), affording a mesoporous bipyridine-based TpBpy COF (Figure 4a). TpBpy was highly crystalline with a high BET surface area of 1667 $m^2 \cdot g^{-1}$ and 2.1 nm pore size (Figure 2b, c). Hence, together with the presence of bipyridine moieties as coordination sites for metal and decent porosity, TpBpy a was perfect host to accommodate electroactive Co species. Upon metalation by impregnation with methanolic cobalt acetate, significant surface area reduction (down to 450 $m^2 \cdot g^{-1}$) and negligible PXRD change were observed, confirming the significant Co–N active sites in the Co-TpBpy (13 wt% of Co deposited). Notably, the electrode of Co-TpBpy-coated glassy carbon exhibited an overpotential of 400 mV at 1 $mA \cdot cm^{-2}$ (calculated to be ~520 mV at 10 $mA \cdot cm^{-2}$) for OER in a phosphate buffer (neutral pH condition) (Figure 4d). More importantly, polarization curve retention was observed even after 1000 cycles, confirming the good stability of the Co-TpBpy electrode. Furthermore, a Tafel slope of 59 $mV \cdot dec^{-1}$ was documented, suggesting possibly that it followed a reversible one-electron transfer mechanism for OER (Figure 4e).[64] It was assumed that these electrocatalytic activities might arise from the synergetic effect of the inherent porosity and the presence of coordinating units in the COF skeleton. For the sake of improving mass transport of the O_2 bubbles during OER, TpBpy was prepared with a hierarchical macro-microporous architecture via a hard-template-assisted method using polystyrene sphere (PS) to better access of the OER active site (Figure 4f).[42] This method allows for the formation of crystalline COFs with inherent macroporosity, thus providing interconnected macropores within the structure (macro-TpBpy) as shown by scanning electron microscopy (SEM) (Figure 4g). In particular, macro-TpBpy managed higher BET surface areas (723 $m^2 \cdot g^{-1}$) relative to the pristine TpBpy (588 $m^2 \cdot g^{-1}$) with preserved pore size, identifying that the macropore efficiently promotes the accessibility of micropores (Figure 4h). Remarkably, upon metalation with cobalt acetate, the macro-TpBpy-Co electrode (mass loading of 0.25 $mg \cdot cm^{-2}$) with a surface area of 387 $m^2 \cdot g^{-1}$ demonstrated a significantly improved OER with a small overpotential of 380 mV to achieve an anodic current density of 10 $mA \cdot cm^{-2}$, which was much smaller than those of macro-TpBpy and the previously reported Co-TpBpy with conventional hydrothermal synthesis (Figure 4i).[41] Furthermore, it exhibited a Tafel slope of 54 $mV \cdot dec^{-1}$, smaller than those of macro-TpBpy (339 $mV \cdot dec^{-1}$), RuO_2 (79 $mV \cdot dec^{-1}$), and the previously reported Co-TpBpy (59 $mV \cdot dec^{-1}$)[41], thus indicating the favorable reaction kinetics in the OER process (Figure 4j). These were assumed due to the homogeneous and interconnected microporous structures of macro-TpBpy.

Adopting similar metal–N as an OER active site, metalloporphyrin with a four coordinated metal–N_4 structure is an attractive OER electrocatalyst; particularly, porphyrin with coordinated high-/low-valent metal ions enables oxidizing/

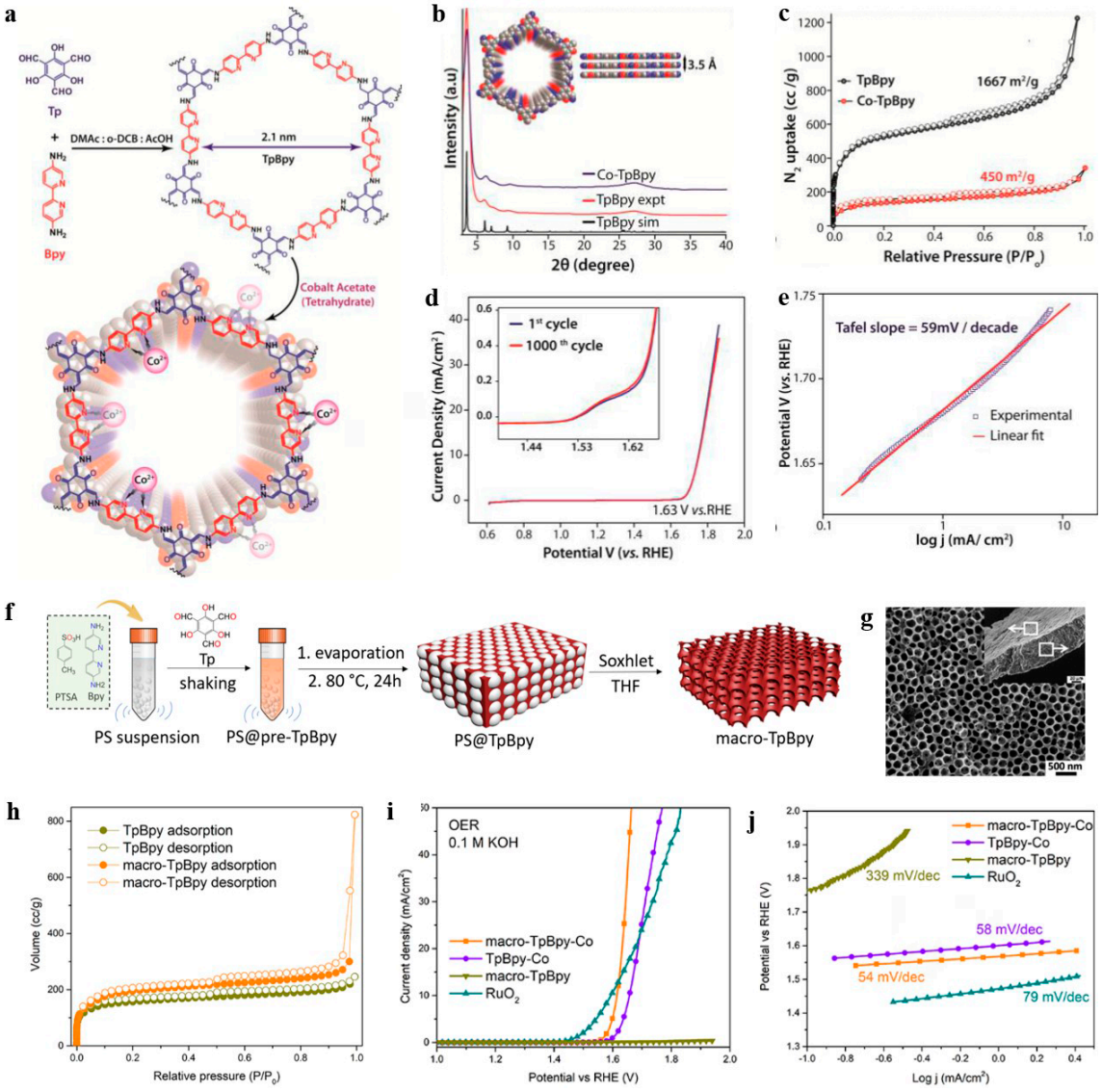

Figure 4 The synthesis and electrocatalytic OER activity Co-TpBPy and macro-TpBPy-Co. (a) Design synthesis of TpBpy and Co-TpBpy via Co (II) impregnation. (b) Comparative PXRD pattern of TpBpy and Co-TpBpy. (c) The N_2 adsorption isotherm of TpBpy and Co-TpBpy. (d) The LSV stability test profile of Co-TpBpy before and after 1000 cycles (inset shows an enlarged view of the LSV profile). (e) The Tafel plot of Co-TpBpy at neutral pH. Reprinted with permission from Ref. 41. Copyright 2016 American Chemical Society. (f) Schematic representation of macro-TpBpy fabrication with PSs as a hard template. (g) SEM image of a monodisperse macro-TpBPy. (h) N_2 adsorption–desorption isotherms of the TpBpy and macro-TpBpy. (i,j) OER polarization curves and the corresponding Tafel plots for macro-TpBpy, macro-TpBpy-Co, TpBpy-Co, and a commercial RuO_2 catalyst. Reprinted with permission from Ref. 42. Copyright 2019 American Chemical Society.

reducing catalytic cycles.[65,66] To this regard, metalloporphyrin-based COFs have been designed to enable OER. For instance, Zeng and team prepared Co-based metalloporphyrin COFs as promising OER electrocatalysts.[43] The COFs were prepared by reacting diarylamine-based 4,4′,4″,4‴-(1,4-phenylenebis(azanetriyl))tetrabenzaldehyde (PATA) or 4,4′,4″,4‴-([1,1′-biphenyl]-4,4′-diylbis(azanetriyl)) tetrabenzaldehyde (BDTA) with 5,10,15,20-tetrakis(4-aminophenyl)porphinato]-cobalt (TAPP(Co)) to afford CoTAPP-PATA-COF and CoTAPP-BDTA-COF, respectively, via one-step synthesis. In particular, these arylamines are typical electron donors and redox-active cores,[67,68] thus they could promote effective electron transport as well as improve the electrochemical active surface areas in the electrocatalytic process. Hence, both Co-based porphyrin COFs are attractive electrocatalysts. In addition, CoTAPP-PATA-COF achieved a

high surface area of 943.72 $m^2 \cdot g^{-1}$ with a pore size of 1.1 nm, while higher surface areas (1047.82 $m^2 \cdot g^{-1}$) and large pore size (1.2 nm) were shown by CoTAPP-BDTA-COF. As for one-step synthesis, Co species were about 3.88 and 3.21 wt% in CoTAPP-PATA-COF and CoTAPP-BDTA-COF, respectively. More importantly, both COFs are chemically stable even in highly acidic or basic solutions. Inspired by these prospective properties, both Co–porphyrin COFs were employed as oxygen-involving electrocatalysts. As for OER in particular, the electrode-based CoTAPP-PATA-COF (mass loading of 0.2 $mg \cdot cm^{-2}$) afforded an overpotential of 420 mV at 10 $mA \cdot cm^{-2}$ current density, which was smaller than that of CoTAPP-BDTA-COF (470 mV). Meanwhile, a small Tafel slope of 56 and 57 $mV \cdot dec^{-1}$ was achieved by CoTAPP-PATA-COF and CoTAPP-BDTA-COF, respectively. On the other hand, higher overpotentials of 670 and 550 mV were observed for both NiTAPP-PATA-COF and FeTAPP-PATA-COF electrode analogues with similar mass loading (0.2 $mg \cdot cm^{-2}$), confirming that Co was more reactive for HER than Ni and Fe. Further investigation revealed that diarylamine units in both COFs played an important role in improving the electrocatalytic performance. On the other hand, to construct COFs with high density and openly exposed OER active sites, Peng and team introduced Co–porphyrin onto a 2-fold interpenetrated 3D structure.[44] A highly connective 3D ZJTU-1 COF with **stp** topology was prepared by condensing 6-connected hexagonal prism (D_{3h}) node-based 2,3,6,7,14,15-hexa(4-formylphenyl)triptycene (HFPTP) with 5,10,15,20-tetra (4-aminophenyl)porphyrin (TAPP) as a perfect support to anchor Co species. Interestingly, only a slight decrease of surface areas (from 724.97 to 656.89 $m^2 \cdot g^{-1}$) and retained pore size were observed after immobilization of 5.54% of Co metal into the porphyrin moieties (ZJTU-1@Co). Remarkably, an electrode composed of ZJTU-1@Co deposited onto a carbon cloth (mass loading of 4 $mg \cdot cm^{-2}$) in 1 M KOH solution only required an overpotential of 295 mV at 10 $mA \cdot cm^{-2}$, which was close to the commercial RuO_2 (257 mV). Additionally, it exhibited a Tafel slope of 64 $mV \cdot dec^{-1}$. This report clearly shows that 3D COFs with their open-pore structure show impressive electrocatalytic performance.

Likewise, phthalocyanine COFs (Pc-COFs) also provide suitable anchor sites for uniformly deposited metal-based electrocatalysts.[69] Recently, Salonen and co-worker designed a series of metalated imide-linked Pc-COFs with well-controlled Ni and Fe species as OER electrocatalysts.[45] The H_2PcCOF, H_2NiPcCOF, and NiPcCOF series were bottom-up prepared by varying the H_2Pc/NiPc ratio to link with benzidine, while controlled postsynthetic modification of the as-synthesized H_2PcCOF and H_2NiPcCOF with a solution of $FeCl_2$ in DMF, afforded H_2FeCOF and H_2NiFeCOF series (Figure 5a). The resultant COFs showed moderate surface areas (467, 462, 323, 326, and 346 $m^2 \cdot g^{-1}$) with almost similar pore sizes (1.2, 1.3, 1.3, 1.4, and 1.4 nm) for H_2PcCOF, H_2NiPcCOF, NiPcCOF, H_2FePcCOF, and H_2NiFePcCOF, respectively. Upon subjecting to the OER electrolysis system, the deposited COFs onto the Ni foam (mass loading of 3 $mg \cdot cm^{-2}$) demonstrated notable OER performance, with NiPcCOF achieved the smallest overpotential of 410 mV (at 10 $mA \cdot cm^{-2}$) relative to other metalated Pc-COFs ($\eta_{10} \approx 430$ mV), while H_2PcCOF showed unfavorable overpotential following the Ni foam (Figure 5b). Furthermore, the metalated PcCOFs also showed much smaller Tafel slopes (62, 68, 75, and 78 $mV \cdot dec^{-1}$ for H_2FePcCOF, H_2NiFePcCOF, NiPcCOF and H_2NiFePcCOF, respectively) than H_2PcCOF (121 $mV \cdot dec^{-1}$) and Ni foam (127 $mV \cdot dec^{-1}$) (Figure 5c). More importantly, the COFs showed excellent long-term stability in 1 M NaOH electrolyte during the tested 100 h (Figure 5d). These results suggest that PcCOFs play a crucial role in improving the electrocatalytic performances and stability of the electrodes. Meanwhile, using different anchoring sites (i.e., $-SO_3$), the bimetallic NiFe ion was incorporated into 2D COF-SO_3 to obtain Ni_xFe_{1-x}@COF-SO_3 as promising OER electrocatalysts.[46] Interestingly, the $Ni_{0.5}Fe_{0.5}$@-COF-SO_3-based electrode showed impressive OER performance with a turnover frequency of 0.14 s^{-1} and a small overpotential of 300 mV at 10 $mA \cdot cm^{-2}$ as well as a Tafel slope of 83 $mV \cdot dec^{-1}$. On another occasion, a 2D COF with tetrazole units (COF-TpDb-TZ) was postsynthetically prepared to accommodate electroactive Co ions to serve as OER electrocatalysts.[47] As predicted, upon metalation, COF-TpDb-TZ-Co only required a overpotential of 390 mV to achieve a current density of 10 $mA \cdot cm^{-2}$ in 1 M KOH solution, which was much lower than that of COF-TpDb-TZ. This strengthens the significant catalytic activity of Co^{2+}. Additionally, it exhibits a Tafel slope of 82 $mV \cdot dec^{-1}$, much smaller than that of COF-TpDb-TZ (477 $mV \cdot dec^{-1}$), thus indicating the faster kinetic and improved electrocatalytic performance of the COF upon metalation.

COFs with M NPs have also been explored as potential OER electrocatalysts. Vaidhyanathan and team in 2016 used an imine-linked COF (IISERP-COF2) with highly flexible tetrahedral sp^3 nitrogen in building (tris(4-formylphenyl)-amine) as a perfect support to stabilize a small size OER active M NP.[48] The highly crystalline IISERP-COF2 managed a high BET surface area of 557 $m^2 \cdot g^{-1}$ and a bimodal pore size of 1.9 and 2.1 nm. The presence of the sp^3 nitrogen triazine core and C=N groups in IISERP-COF2 enhanced interaction towards formation of M NPs. Metalation was performed via the solution route and reduction to M^0 using $NaBH_4$ to afford series of M NPs loaded with 16Ni-COF [**1**], 16Co-COF [**2**], 8Co:8Ni-COF [**3**], 12Co:4Ni-COF [**4**], and 4Co:12Ni-COF [**5**], causing almost 71% porosity reduction. An electrocatalytic OER experiment in deaerated 0.1 M KOH with a catalyst mass loading of 20 µg confirmed that the composite **5** exhibited excellent OER electrocatalytic activity with an overpotential of ≈ 258 mV at 10 $mA \cdot cm^{-2}$, superior to **3** (315.8 mV), **4** (399.8 mV), **1** (402.3 mV) and **2** (487.3 mV) as well as to all

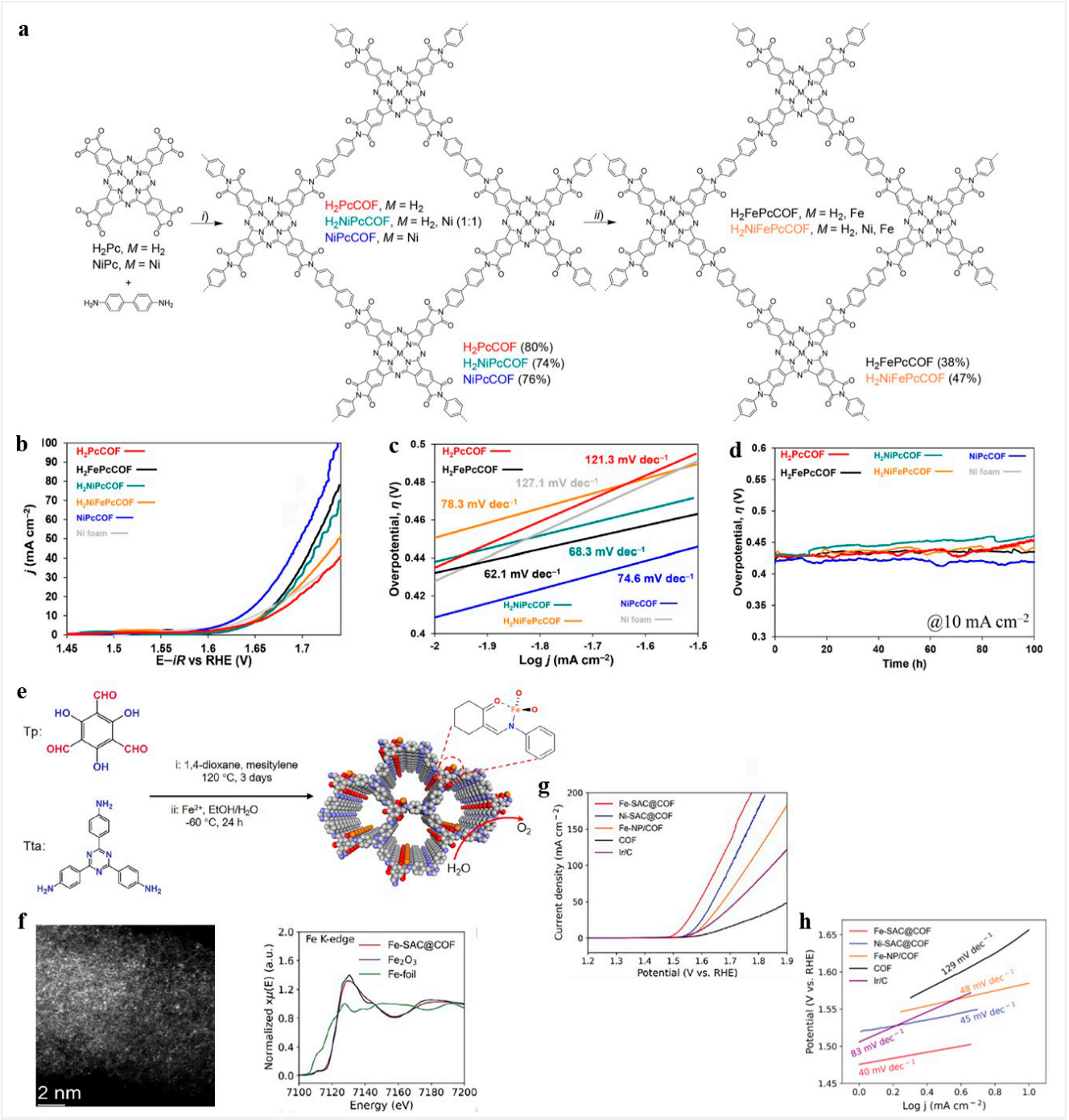

Figure 5 Design synthesis and electrocatalytic OER performance of metalated Pc-COFs series. (a) Synthesis route to H_2PcCOF and metalated PcCOFs. (b) Anodic polarization curves of H_2PcCOF and metalated PcCOF electrodes in 1 M NaOH electrolyte. (c) The Tafel plots for H_2PcCOF and metalated PcCOFs. (d) Chronopotentiometry profiles of H_2PcCOF and metalated PcCOFs at 10 mA · cm^{-2}. Reprinted from Ref. 45 published under a creative commons license (CC BY). (e) The schematic diagram of the fabrication process for Fe-SAC@COF. (f) The aberration-corrected HAADF-STEM images of Fe-SAC@COF (left) and the corresponding experimental K-edge XANES spectra and the reference samples (right). (g) The LSV curve comparison of the M-SAC@COF. (h) The Tafel slope comparison of M-SAC@COF. Reprinted from Ref. 50 published under a creative commons license (CC BY-NC-ND).

reported OER-based COF electrocatalysts (Table 1). Likewise, the composite **5** showed the smallest Tafel slope (39.8 $mV \cdot dec^{-1}$) compared to **4** (86.3 $mV \cdot dec^{-1}$), **3** (64.1 $mV \cdot dec^{-1}$), **2** (94.1 $mV \cdot dec^{-1}$), and **1** (89.4 $mV \cdot dec^{-1}$). Employing low band-gap benzimidazole-linked IISERP-COF3 as a support, Vaidhyanathan and team further deposited Ni_3N NP to enhance the electrocatalytic performance of this transition metal catalyst.[49] Such COFs with heterocyclic linkage could drive a low band gap due to the higher conjugation, thus possessing an ideal electronic support for catalytically active NPs.[70] IISERP-COF3 was highly porous with a BET surface area of 2022 $m^2 \cdot g^{-1}$ and mesopores of 2.5 nm, hence favoring the growth of metallic Ni_3N NPs via nanoscopic confinement (Ni_3N-IISERP-COF3). More importantly, the conducting nature of the COF allows electronic interaction among COF/Ni_3N possible. Accordingly, electrodes based on IISERP-COF3 or Ni_3N-IISERP-COF3 were prepared by depositing them onto glassy carbon electrodes with a mass loading of ~0.07 $mg \cdot cm^{-2}$. Interestingly, Ni_3N-IISERP-COF3 with sufficient porosity preservation (~606 $m^2 \cdot g^{-1}$) afforded an overpotential of 230 mV at 10 $mA \cdot cm^{-2}$, smaller than that of pristine IISERP-COF3 (400 mV) in deaerated 1 M KOH solution. Additionally, it exhibited a Tafel slop of 79 $mV \cdot dec^{-1}$. These noticeable electrocatalytic performances were assumed as the COF acted as a reliable matrix to disperse Ni_3N NPs with higher accessibility, thus providing effective charge transport within the composite. To maximize the atomic-utilization efficiency, an iron single-atom catalyst (Fe SAC) confined in a 2D COF was realized as a powerful OER electrocatalyst.[50] A 2D COF (Tp-Tta COF) was designed with a suitable coordination pocket to confine OER active Fe-SAC via unusual Fe–NO atomic arrangement in the skeleton (Figure 5e). The Tp-Tta COF was a typical 1 nm honeycomb-like pore COF with a BET surface area of 716 $m^2 \cdot g^{-1}$ and excellent chemical stability even in alkaline solution. Deposition of Fe-SAC was performed by mixing the COF with a Fe precursor at low temperature (−60 °C) to prevent metal aggregation and further reduction treatment with $N_2H_4.H_2O$ to produce the targeted Fe-SAC@COF. This procedure deposited 1.0 wt% Fe-SAC as confirmed by its TEM image and K-edge XANES spectrum (Figure 5f), thus causing reduction of surface areas (down to 470 $m^2 \cdot g^{-1}$) without affecting the pore size. Hence, Fe-SAC@COF is an attractive electrocatalyst. As predicted, an electrode composed of Fe-SAC@COF (catalyst mass loading up to 1 $mg \cdot cm^{-2}$) exhibited excellent OER activity with a low overpotential of 290 mV to achieve a current density of 10 $mA \cdot cm^{-2}$, which was superior compared with the prepared Fe-NP/COF (359 mV) and pristine Tp-Tta COF electrode (430 mV) (Figure 5g). Additionally, it also outperformed the Ni-SAC@COF analog (337 mV) prepared via the same procedure. This result was further amplified by its fastest kinetics for OER proven by its lowest Tafel slope (40 $mV \cdot dec^{-1}$) among all samples (45, 51, and 129 $mV \cdot dec^{-1}$ for Ni-SAC@COF, Fe-NP/COF, and Tp-Tta COF, respectively) (Figure 5h). This work provides evidence that improving the atomic utilization by means of SA species improved the electrocatalytic performance.

Although OER is sluggish and thus required metal catalysts, metal-free COFs are also potential OER electrocatalysts. A new electroactive thiadiazole-based COF (C4-SHz COF) was developed as a promising OER electrocatalyst by reacting 1,3,5-tris(4-formylphenyl)benzene with 2,5-dihydrazinyl-1,3,4-thiadiazole.[51] Upon activation with supercritical CO_2 treatment, the C4-SHz COF was highly crystalline and composed of a nitrogen-rich thiadiazole moiety as an OER active site with a BET surface area of 1224 $m^2 \cdot g^{-1}$ and an accessible pore size of mainly 1.85 nm. These properties suggest a potential electrocatalyst application. Accordingly, the OER activity of a prepared electrode of C4-SHz COF with a mass loading of 0.07 $mg \cdot cm^{-2}$ was tested in aqueous 1 M KOH solution. Remarkably, the COF exhibited an onset overpotential of 250 mV and only required an overpotential of 320 mV to reach a current density of 10 $mA \cdot cm^{-2}$, which was lower than that of commercial IrO_2/C catalyst. Comparatively, this performance is outstanding in comparison with several metalated-COF-based OER electrocatalysts mentioned in Table 1. Furthermore, it managed a Tafel slope of 39 $mV \cdot dec^{-1}$, lower than that of IrO_2/C (57 $mV \cdot dec^{-1}$) tested in the same system. Further electrochemical analysis confirmed that this notable OER performance may associate with the higher charge transfer kinetics and faster electron transfer process within the structures of the COF. Inspired by our previous result on tetrathiafulvalene (TTF)-based 3D COFs with excellent electrical conductivity,[71] our team recently designed a 2D TTF-COF (JUC-630) as a potential metal-free COF OER electrocatalyst taking advantage of the good electron donor of TTF and thiadiazole unit as an OER active site. JUC-630 was a mesopore COF with a pore diameter of 2.35 nm and achieved a surface area of 907 $m^2 \cdot g^{-1}$, thus providing accessibility to the electrocatalytic sites. It was then employed as an electrocatalyst for water oxidation in aqueous 1 M KOH solution. An overpotential of 400 mV was required to achieve a current density of 10 $mA \cdot cm^{-2}$, which was smaller than the overpotential required by Etta-Td (450 mV), a COF analogue without the TTF unit. This result confirms the crucial role of TTF unit in the OER performance of the COF. Additionally, it exhibited a Tafel slope of 104 $mV \cdot dec^{-1}$.

4 Conclusions and Outlook

Owing to their prominent properties such as high crystallinity, superior porosity with devisable porous architecture and tunable chemical composition and functionality, COFs have been attractive new-generation electrocatalytic materials, particularly for water splitting electrocatalysis. COFs

offer several benefits in comparison with traditional electrocatalytic materials, such as controllable heteroatom incorporation and designed porous architectures, thus enhancing the catalytic performance. The exceptional structural stability is reinforced by additional supramolecular forces and the complementary donor/acceptor and redox units, enriching their electronic characters. Furthermore, COFs provide a suitable platform for incorporating reactive metals via strong coordination chemistry, resulting in excellent and highly efficient electrocatalysts. These advantages result in advancement in the employment of COFs as water splitting electrocatalysts. Among them, noble metals containing COFs have been prepared to improve the selectivity and stability of the noble metals. Meanwhile, in terms of low cost and decent electrocatalytic performance, non-noble metal/COF electrocatalysts, including dual transition metals and SAC-containing COFs, have been widely explored as promising electrocatalysts. Nevertheless, metal-free COFs have also been screened recently, envisioning a green and sustainable approach for water splitting technology.

Although some progresses have been seen, the research of COFs in this field is still in its infancy. Thus, there are still lot of gaps for improvements. Certainly, some challenges are there to be addressed for the sake of efficient water splitting electrocatalysis. Generally, COFs are less conductive, thus it is highly important to optimize the conductivity by means of specific design of COF structure, such as with a donor–acceptor configuration. In the case of durability, COF-based electrocatalysts shall be highly resistant toward harsh environments (e.g., in strong acidic and basic systems). This could be tackled by employing COFs with stable linkages or introduction of supramolecular enforcement within the structure. Meanwhile, most of those COF electrocatalysts are dominated by 2D COF structures, which are likely to suffer from ineffective active site utilization due to the highly layer stacking. 3D COF electrocatalysts shall provide an efficient platform with 3D open-pore structures and higher surface areas. Despite highly significant to boost the electrocatalytic activity, development of single-atom-based water splitting electrocatalysts is still rare. Designing COFs with specific coordination pockets has been seen to enable the controlled nucleation of single-atom species. Furthermore, development of dual HER/OER electrocatalyst-based COFs is unseen and yet challenging to realize. A rational design of such electrocatalysts is highly in demand to promote full water splitting electrocatalysis. Nevertheless, the use of thin film or membrane-based COFs, instead of commonly prepared crystalline powder, provides convenience for integration into the device. Finally, the role of COFs in the catalytic process is still unclear. Thus, it is highly important to get insight into the active site and chemical kinetics at the molecular level. In summary, by addressing all these synthetic and practical challenges, COF-based electrocatalysts would be highly promising for the development of efficient and low-cost water splitting technology.

Funding Information

This work was supported by the National Key R&D Program of China (2021YFF0 500 504 and 2022YFB3 704 900), the National Natural Science Foundation of China (22 025 504, 21 621 001, and 22 105 082), the SINOPEC Research Institute of Petroleum Processing, “111” project (BP0719036 and B17020), and the program for JLU Science and Technology Innovative Research Team. Y. Y. and F. C. thank Jilin University “Dingxin Scholar Program” for the financial support.

Conflict of Interest

The authors declare no conflict of interest.

References

(1) Aricò, A. S.; Bruce, P.; Scrosati, B.; Tarascon, J.; van Schalkwijk, W. *Nat. Mater.* **2005**, *4*, 366.
(2) Zou, X.; Zhang, Y. *Chem. Soc. Rev.* **2015**, *44*, 5148.
(3) Jin, H.; Guo, C.; Liu, X.; Liu, J.; Vasileff, A.; Jiao, Y.; Zheng, Y.; Qiao, S. Z. *Chem. Rev.* **2018**, *118*, 6337.
(4) Walter, M. G.; Warren, E. L.; McKone, J. R.; Boettcher, S. W.; Mi, Q.; Santori, E. A.; Lewis, N. S. *Chem. Rev.* **2010**, *110*, 6446.
(5) Hisatomi, T.; Kubota, J.; Domen, K. *Chem. Soc. Rev.* **2014**, *43*, 7520.
(6) Jiao, Y.; Zheng, Y.; Jaroniec, M.; Qiao, S. Z. *Chem. Soc. Rev.* **2015**, *44*, 2060.
(7) Antolini, E. *ACS Catal.* **2014**, *4*, 1426.
(8) Lee, Y.; Suntivich, J.; May, K. J.; Perry, E. E.; Shao-Horn, Y. *J. Phys. Chem. Lett.* **2012**, *3*, 399.
(9) Cui, X.; Gao, L.; Lei, S.; Liang, S.; Zhang, J.; Sewell, C. D.; Xue, W.; Liu, Q.; Lin, Z.; Yang, Y. *Adv. Funct. Mater.* **2021**, *31*, 2009197.
(10) Wang, H.; Liu, R.; Li, Y.; Lü, X.; Wang, Q.; Zhao, S.; Yuan, K.; Cui, Z.; Li, X.; Xin, S.; Zhang, R.; Lei, M.; Lin, Z. *Joule* **2018**, *2*, 337.
(11) Gao, D.; Guo, J.; Cui, X.; Yang, L.; Yang, Y.; He, H.; Xiao, P.; Zhang, Y. *ACS Appl. Mater. Interfaces* **2017**, *9*, 22420.
(12) Yang, Y.; Zhou, M.; Guo, W.; Cui, X.; Li, Y.; Liu, F.; Xiao, P.; Zhang, Y. *Electrochim. Acta* **2015**, *174*, 246.
(13) Zhao, X.; Yang, Y.; Li, Y.; Cui, X.; Zhang, Y.; Xiao, P. *J. Mater. Sci.* **2016**, *51*, 3724.
(14) Cui, X.; Xiao, P.; Wang, J.; Zhou, M.; Guo, W.; Yang, Y.; He, Y.; Wang, Z.; Yang, Y.; Zhang, Y.; Lin, Z. *Angew. Chem. Int. Ed.* **2017**, *56*, 4488.
(15) Zhang, J.; Zhao, Z.; Xia, Z.; Dai, L. *Nat. Nanotechnol.* **2015**, *10*, 444.
(16) Peng, P.; Zhou, Z.; Guo, J.; Xiang, Z. *ACS Energy Lett.* **2017**, *2*, 1308.
(17) Xiang, Z.; Xue, Y.; Cao, D.; Huang, L.; Chen, J. F.; Dai, L. *Angew. Chem. Int. Ed.* **2014**, *53*, 2433.
(18) Côté, A. P.; Benin, A. I.; Ockwig, N. W.; O'Keeffe, M.; Matzger, A. J.; Yaghi, O. M. *Science* **2005**, *310*, 1166.
(19) Waller, P. J.; Gándara, F.; Yaghi, O. M. *Acc. Chem. Res.* **2015**, *48*, 3053.
(20) Ji, C.; Su, K.; Wang, W.; Chang, J.; El-Sayed, E. S. M.; Zhang, L.; Yuan, D. *CCS Chem.* **2022**, *41*, 3094.

(21) Yusran, Y.; Li, H.; Guan, X.; Fang, Q.; Qiu, S. *EnergyChem* **2020**, *2*, 100035.
(22) Yusran, Y.; Fang, Q.; Valtchev, V. *Adv. Mater.* **2020**, *32*, 2002038.
(23) Sun, J.; Xu, Y.; Lv, Y.; Zhang, Q.; Zhou, X. *CCS Chem*. **2023**, *5*, 1259.
(24) Ding, S.-Y.; Wang, W. *Chem. Soc. Rev.* **2013**, *42*, 548.
(25) Wan, S.; Gándara, F.; Asano, A.; Furukawa, H.; Saeki, A.; Dey, S. K.; Liao, L.; Ambrogio, M. W.; Botros, Y. Y.; Duan, X.; Seki, S.; Stoddart, J. F.; Yaghi, O. M. *Chem. Mater.* **2011**, *23*, 4094.
(26) Zhang, C. R.; Cui, W. R.; Xu, R. H.; Chen, X. R.; Jiang, W.; Wu, Y. Di; Yan, R. H.; Liang, R. P.; Qiu, J. D. *CCS Chem*. **2021**, *3*, 168.
(27) Liu, Y.; Ren, J.; Wang, Y.; Zhu, X.; Guan, X.; Wang, Z.; Zhou, Y.; Zhu, L.; Qiu, S.; Xiao, S.; Fang, Q. *CCS Chem*. **2023**, *5*, 2033.
(28) Suen, N. T.; Hung, S. F.; Quan, Q.; Zhang, N.; Xu, Y. J.; Chen, H. M. *Chem. Soc. Rev.* **2017**, *46*, 337.
(29) Wu, Y.; Veleta, J. M.; Tang, D.; Price, A. D.; Botez, C. E.; Villagrán, D. *Dalton Trans*. **2018**, *47*, 8801.
(30) Conway, B. E.; Tilak, B. V. *Electrochim. Acta* **2002**, *47*, 3571.
(31) Man, I. C.; Su, H. Y.; Calle-Vallejo, F.; Hansen, H. A.; Martínez, J. I.; Inoglu, N. G.; Kitchin, J.; Jaramillo, T. F.; Nørskov, J. K.; Rossmeisl, J. *ChemCatChem* **2011**, *3*, 1159.
(32) Danilovic, N.; Subbaraman, R.; Chang, K. C.; Chang, S. H.; Kang, Y. J.; Snyder, J.; Paulikas, A. P.; Strmcnik, D.; Kim, Y. T.; Myers, D.; Stamenkovic, V. R.; Markovic, N. M. *J. Phys. Chem. Lett*. **2014**, *5*, 2474.
(33) Diercks, C. S.; Yaghi, O. M. *Science* **2017**, *355*, eaal1585.
(34) Guan, X.; Li, H.; Ma, Y.; Xue, M.; Fang, Q.; Yan, Y.; Valtchev, V.; Qiu, S. *Nat. Chem*. **2019**, *11*, 587.
(35) Bhunia, S.; Das, S. K.; Jana, R.; Peter, S. C.; Bhattacharya, S.; Addicoat, M.; Bhaumik, A.; Pradhan, A. *ACS Appl. Mater. Interfaces* **2017**, *9*, 23843.
(36) Yue, J.; Ding, X.; Song, L.; Wang, Y.; Yang, P.; Ma, Y.; Tang, B. *Microporous Mesoporous Mater*. **2022**, *344*, 112169.
(37) Zhou, D.; Tan, X.; Wu, H.; Tian, L.; Li, M. *Angew. Chem. Int. Ed*. **2019**, *58*, 1376.
(38) Zhao, Y.; Liang, Y.; Wu, D.; Tian, H.; Xia, T.; Wang, W.; Xie, W.; Hu, X.; Tian, X.; Chen, Q. *Small* **2022**, *18*, 2107750.
(39) Sun, X.; Hu, Y.; Fu, Y.; Yang, J.; Song, D.; Li, B.; Xu, W.; Wang, N. Small **2023**, in press; doi: 10.1002/smll.202305978
(40) Bai, Y.; Liu, Y.; Liu, M.; Wang, X.; Shang, S.; Gao, W.; Du, C.; Qiao, Y.; Chen, J.; Dong, J.; Liu, Y. *Angew. Chem. Int. Ed*. **2022**, *61*, e202113067.
(41) Aiyappa, H. B.; Thote, J.; Shinde, D. B.; Banerjee, R.; Kurungot, S. *Chem. Mater*. **2016**, *28*, 4375.
(42) Zhao, X.; Pachfule, P.; Li, S.; Langenhahn, T.; Ye, M.; Schlesiger, C.; Praetz, S.; Schmidt, J.; Thomas, A. *J. Am. Chem. Soc*. **2019**, *141*, 6623.
(43) Liu, M.; Liu, S.; Cui, C.; Miao, Q.; He, Y.; Li, X.; Xu, Q.; Zeng, G. *Angew. Chem. Int. Ed*. **2022**, *61*, e202213522.
(44) Gong, C.; Yang, X.; Wei, X.; Dai, F.; Zhang, T.; Wang, D.; Li, M.; Jia, J.; She, Y.; Xu, G.; Peng, Y. *Mater. Chem. Front*. **2022**, *7*, 230.
(45) Jarju, J. J.; Díez, A. M.; Frey, L.; Sousa, V.; Carbó-Argibay, E.; Gonçalves, L. P. L.; Medina, D. D.; Lebedev, O. I.; Kolen'ko, Y. V.; Salonen, L. M. *Mater. Today Chem*. **2022**, *26*, 101032.
(46) Gao, Z.; Gong, L. Le; He, X. Q.; Su, X. M.; Xiao, L. H.; Luo, F. *Inorg. Chem*. **2020**, *59*, 4995.
(47) Liang, Y.; Xia, T.; Wu, Z.; Yang, Y.; Li, Y.; Sui, Z.; Li, C.; Fan, R.; Tian, X.; Chen, Q. *Mater. Today Chem*. **2022**, *24*, 100777.
(48) Mullangi, D.; Dhavale, V.; Shalini, S.; Nandi, S.; Collins, S.; Woo, T.; Kurungot, S.; Vaidhyanathan, R. *Adv. Energy Mater.* **2016**, *6*, 1600110.
(49) Nandi, S.; Singh, S. K.; Mullangi, D.; Illathvalappil, R.; George, L.; Vinod, C. P.; Kurungot, S.; Vaidhyanathan, R. *Adv. Energy Mater.* **2016**, *6*, 1601189.
(50) Wang, X.; Sun, L.; Zhou, W.; Yang, L.; Ren, G.; Wu, H.; Deng, W. Q. *Cell Rep. Phys. Sci*. **2022**, *3*, 100804.
(51) Mondal, S.; Mohanty, B.; Nurhuda, M.; Dalapati, S.; Jana, R.; Addicoat, M.; Datta, A.; Jena, B. K.; Bhaumik, A. *ACS Catal*. **2020**, *10*, 5623.
(52) Xia, W.; Ji, C.; Wang, R.; Qiu, S.; Fang, Q. *Acta Phys. Chim. Sin*. **2023**, *39*, 2212057.
(53) Celebi, K.; Buchheim, J.; Wyss, R. M.; Droudian, A.; Gasser, P.; Shorubalko, I.; Kye, J. Il; Lee, C.; Park, H. G. *Science* **2014**, *344*, 289.
(54) Morales-Guio, C. G.; Stern, L. A.; Hu, X. *Chem. Soc. Rev.* **2014**, *43*, 6555.
(55) Gao, W. Y.; Chrzanowski, M.; Ma, S. *Chem. Soc. Rev.* **2014**, *43*, 5841.
(56) Chen, Y.; Hoang, T.; Ma, S. *Inorg. Chem*. **2012**, *51*, 12600.
(57) Geng, K.; He, T.; Liu, R.; Tan, K. T.; Li, Z.; Tao, S.; Gong, Y.; Jiang, Q.; Jiang, D. *Chem. Rev.* **2020**, *120*, 8814.
(58) Kuhn, P.; Antonietti, M.; Thomas, A. *Angew. Chem. Int. Ed*. **2008**, *47*, 3450.
(59) Hug, S.; Stegbauer, L.; Oh, H.; Hirscher, M.; Lotsch, B. V. *Chem. Mater*. **2015**, *27*, 8001.
(60) Qiao, S.; Zhang, B.; Li, Q.; Li, Z.; Wang, W.; Zhao, J.; Zhang, X.; Hu, Y. *ChemSusChem* **2019**, *12*, 5032.
(61) Chen, X.; Yu, K.; Shen, Y.; Feng, Y.; Zhu, Z. *ACS Appl. Mater. Interfaces* **2017**, *9*, 42139.
(62) Reier, T.; Oezaslan, M.; Strasser, P. *ACS Catal*. **2012**, *2*, 1765.
(63) Blakemore, J. D.; Crabtree, R. H.; Brudvig, G. W. *Chem. Rev.* **2015**, *115*, 12974.
(64) Han, A.; Chen, H.; Sun, Z.; Xu, J.; Du, P. *Chem. Commun*. **2015**, *51*, 11626.
(65) Shaik, S.; Hirao, H.; Kumar, D. *Acc. Chem. Res*. **2007**, *40*, 532.
(66) Lin, C.; Zhang, L.; Zhao, Z.; Xia, Z. *Adv. Mater*. **2017**, *29*, 1606635.
(67) Gong, L.; Yang, X.; Gao, Y.; Yang, G.; Yu, Z.; Fu, X.; Wang, Y.; Qi, D.; Bian, Y.; Wang, K.; Jiang, J. *J. Mater. Chem. A* **2022**, *10*, 16595.
(68) Gu, S.; Hao, R.; Chen, J.; Chen, X.; Liu, K.; Hussain, I.; Liu, G.; Wang, Z.; Gan, Q.; Guo, H.; Li, M.; Zhang, K.; Lu, Z. *Mater. Chem. Front*. **2022**, *6*, 2545.
(69) Urbani, M.; Ragoussi, M.-E.; Nazeeruddin, M. K.; Torres, T. *Coord. Chem. Rev.* **2019**, *381*, 1.
(70) Xu, Y.; Jin, S.; Xu, H.; Nagai, A.; Jiang, D. *Chem. Soc. Rev.* **2013**, *42*, 8012.
(71) Li, H.; Chang, J.; Li, S.; Guan, X.; Li, D.; Li, C.; Tang, L.; Xue, M.; Yan, Y.; Valtchev, V.; Qiu, S.; Fang, Q. *J. Am. Chem. Soc*. **2019**, *141*, 13324.